Stadium billiard with moving walls

Doron Cohen[1] and Diego A. Wisniacki[2]

[1]*Department of Physics, Ben-Gurion University, Beer-Sheva 84105, Israel*
[2]*Departamento de Física "J.J. Giambiagi," FCEN-UBA, Pabellón 1, Ciudad Universitaria, 1428 Buenos Aires, Argentina*

We study the evolution of the energy distribution for a stadium with moving walls. We consider a one period driving cycle, which is characterized by an amplitude A and a wall velocity V. This evolving energy distribution has both "parametric" and "stochastic" components. The latter are important for the theory of quantum irreversibility and dissipation in driven mesoscopic devices. For an extremely slow wall velocity V, the spreading mechanism is dominated by transitions between neighboring levels, while for larger (nonadiabatic) velocities, the spreading mechanism has both perturbative and nonperturbative features. We present a numerical study which is aimed at identifying the latter features. A procedure is developed for the determination of the various V regimes. The possible implications of linear response theory are discussed.

I. INTRODUCTION

Consider the problem of a particle in a box, where some piece of the wall is deformed periodically in time. As an example, one may think of a particle in a cylinder with a moving piston. The particle has mass m and kinetic energy E. The piston is pushed back and forth. The velocity in which the piston is displaced is $\pm V$ and the maximum displacement is A. At the end of each cycle, the piston is back in its original location.

In the present paper, we are going to study what happens to a quantum-mechanical particle in such a box, during one cycle of the driving. We assume that the particle is initially prepared in an energy eigenstate of the (undeformed) box. We shall explain that it is important to specify whether the maximum displacement A is lesser or greater compared with the de Broglie wavelength.

The problem of a particle in a box with a moving wall is a prototype example for study of driven systems [1] which are described by a Hamiltonian $\mathcal{H}(x(t))$, where $x(t)$ is a time dependent parameter. In the case of a piston, the parameter x is the position of the piston, and we use the notation $V = |\dot{x}|$.

There is a lot of interest today in studies of quantum irreversibility. This is an issue relevant to the design of quantum computers, where the fidelity of a driving cycle is important. If at the end of a driving cycle, the system is back in its initial state, then we say that the driving cycle has high fidelity. Obviously, the piston model can serve as a prototype example for studying of quantum irreversibility [2].

The study of one-cycle driving also constitutes a bridge to the study of the response to multicycle (periodic) driving. It should be clear that the long time behavior of driven systems is determined by the short time dynamics. Therefore, it is essential to have a good understanding of the latter.

At first sight, one may think that it is simple to study the one-dimensional (1D) box case, also known as "infinite square well potential with moving wall" [3,4]. The case of periodic driving is also known as the "Fermi acceleration problem" [5]. At a second sight, one finds out that the 1D-box case is actually the most complicated one. As in the case of the kicked rotator (standard map) [6,8,9], there is a complicated route to chaos and stochasticity.

Things become much simpler if the motion in the box is chaotic to begin with. Driven chaotic systems exhibit, as a result of the driving, stochastic energy spreading of a relatively simple nature [1]. This is the case that we want to consider in this paper. Hence, we consider the simplest "chaotic box," which is a 2D "billiard" model. Specifically, we are going to introduce a detailed numerical study of the *one-pulse response of a stadium billiard to a shape deformation*. The stadium billiard is a recognized prototype system for "quantum chaos" studies. Our simulations are feasible, thanks to a new powerful technique for finding clusters of billiard eigenstates [7,10,11]. Previous applications of this technique, to the study of restricted aspects of the present problem, have been reported in Refs. [12,13].

The work that is presented in this paper is a numerical study which is aimed at presenting a systematic analysis of nonperturbative features of a *time dependent* spreading process [14–16]. A procedure is developed for the determination of the various time stages in the evolution of the energy distribution. This allows the identification of the various V regimes ("adiabatic," "perturbative," "nonperturbative," and "sudden"), which were predicted in past theoretical studies.

II. OUTLINE

In Secs. III and IV, we define the model system, and briefly describe the classical picture. In particular, we explain that the *time dependent features* which we study in this paper are purely quantum mechanical, and not of semiclassical origin.

In Sec. V, we define the main objective of our study, which is the energy spreading kernel $P_t(n|m)$. See Eq. (4). Regarded as a function of the level index n, it is the energy distribution after time t, while m is the initial level. We also define the square root of the variance $\delta E(t)$ and the 50% probability width $\Gamma(t)$, which characterize the evolving energy distribution.

Our three-phase strategy for analysis of energy spreading is presented in Sec. VI. The three phases are as follows:

(I) Study of the band profile.
(II) Study of parametric evolution.
(III) Study of the actual time evolution.

The relevant information regarding "phase I" is summarized in Sec. VII. Various approximations for $P_t(n|m)$ and, in particular, the notion of "parametric evolution" are presented in Sec. VIII. The relevant information regarding "phase II" is summarized in Sec. IX. The main concern of this paper is "phase III."

For a given V, one should be able to characterize the nature of the dynamical scenario. The theoretical considerations regarding this issue have been discussed in Refs. [17,14–16], and for a concise review see Ref. [2]. Rather than duplicating these discussions, we are going to present in Sec. X a phenomenological definition, and a practical procedure, for the identification of the V regimes. We would like to emphasize that here the different dynamical scenarios (corresponding to the different V regimes) are illustrated in a numerical simulation. The only other numerical studies (mainly Refs. [15,12]) were too restricted in scope, and did not contain analysis of the stages in the evolution of the energy *distribution*.

Sections XI and XII question the applicability of linear response theory (LRT) to the analysis of the energy spreading. Further discussion on nonperturbative response and conclusions are presented in Sec. XIII.

III. THE SEMICLASSICAL PICTURE

Consider a *classical particle* inside a box. Its kinetic energy is E and the corresponding velocity is $v_E = \sqrt{2E/m}$. The shape of the box is externally controlled. The control parameter is denoted by x. We assume that x has units of length, such that $V = |\dot{x}|$ is the typical wall velocity. Obviously, different parts of the wall may have different velocities. In case of the "piston model," only one piece of the wall is moving (either inward or outward). However, we are not interested in the trivial *conservative* work which is being done, but only in the *irreversible* work. Therefore, rather than analyzing an actual piston model configuration, it is wiser to consider a *volume preserving* deformation. In such a case, the conservative work is zero, and the major issue is the irreversible effect that is explained below.

As a result of the collisions of the particle with the deforming walls, there is a stochasticlike diffusion in energy space. The explanation is as follows: Each time that the particle collides with the moving wall, it either gains or loses energy. To simplify the presentation, let us assume head-on collisions. The change in energy is $\pm 2m v_E V$ depending on whether the wall is moving inward or outward at the point of the collision. For volume preserving deformation, the ergodic average over δE gives zero. Thus, we have random walk in energy space where the steps are $\pm 2m v_E V$. This leads to diffusion in energy space. As explained in Ref. [16], this diffusion is biased (the diffusion is stronger for larger E). This leads, in the long run, to a systematic (irreversible)

increase of the average energy. For a more detailed presentation that takes the box geometry into account, see Ref. [18].

Do we have a corresponding (semiclassical) picture in the quantum-mechanical case? Again, we remind the reader that we assume a volume preserving deformation. This implies that the energy levels of the system do not have a collective upward or downward change as a result of the deformation. The physics in which we are interested is related to the transitions between different levels. The question that we ask is whether these transitions are "classical-like."

Let us assume that we start with an eigenstate whose energy is E. Semiclassically, it is as if we start with a microcanonical preparation. If the dynamics is of classical nature, then we expect that after a short time, some of the probability will make a transition $E \mapsto E'$ such that $|E' - E| \sim 2m v_E V$. Naturally, such description is meaningful only if the energy scale $2m v_E V$ is much larger than the mean-level spacing. This leads for 1D box to the condition

$$V > \hbar/mL. \tag{1}$$

In the general case (e.g., 2D box), having $2m v_E V$ much larger than the mean-level spacing is *not* a sufficient condition for getting semiclassical behavior. Still, nontrivial analysis [19] reveals that the condition for getting semiclassical spreading in the general case is the same as in the 1D case, namely, given by Eq. (1).

The above Eq. (1) is a necessary condition for having semiclassical transitions. In order to actually *witness* semiclassical transitions, it is also necessary to have a time period much larger compared with the ballistic time ($A/V \gg L/v_E$), and to have an amplitude that is much larger compared with the de Broglie wavelength [$A \gg \hbar/(m v_E)$]. These additional conditions can be satisfied only in the *semiclassical regime*, which is defined by Eq. (1), else they are not compatible.

IV. THE NUMERICAL MODEL

As a specific example for chaotic box, we consider the quarter stadium billiard. We define x as the length of the straight edge, and adjust the radius parameter such that the total area is kept constant. For numerical reasons, we do not analyze this model "literally" but rather consider, as in previous study [12], a linearized version of the quarter stadium billiard Hamiltonian. Namely, we study a model Hamiltonian that has the matrix representation

$$\mathcal{H}(x(t)) \mapsto \mathbf{E} + \delta x(t) \mathbf{F}. \tag{2}$$

Here, $\mathbf{E}$ is an ordered diagonal matrix that consists of the eigenenergies E_n of the quarter stadium billiard with straight edge $x = 1$. The eigenenergies were determined numerically. The perturbation due to δx deformation is represented by the matrix $\mathbf{F}$. Also this matrix has been determined numerically as explained in Ref. [12]. We note that the fingerprints of the classical chaos are present in the statistical properties of the matrices $\mathbf{E}$ (level statistics) and $\mathbf{F}$ (band structure). The latter is discussed in Sec. VII.

The *linearization* [Eq. (2)] of the billiard Hamiltonian can be regarded as a valid *approximation* if the wall displacement parameter δx is small as compared with the de Broglie wavelength. This automatically excludes the possibility of addressing the semiclassical regime, which has been discussed in the preceding section. In our simulation, the de Broglie wavelength is roughly 0.1. This implies that (at best) the maximum driving amplitude that can be allowed is $A = 0.2$, so as to have $|\delta x(t)| < 0.1$. [Note that for presentation purposes, we later redefine $\delta x(t)$ as $\delta x(t) - \delta x(0)$]. In the simulations we indeed have $A = 0.2$, meaning that we allow a deformation that is comparable or possibly somewhat larger than that "allowed" by the linearization.

However, in spite of the fact that Eq. (2) may be a "bad" or even an "inadequate" approximation to real-world physics, it is still a totally "legitimate" Hamiltonian from mathematical point of view. Moreover, the numerical model Eq. (2) contains all the *physical* ingredients that are relevant for the aim of the present study.

To summarize, in this paper we consider, as far as formulation is concerned, a chaotic billiard driven by volume preserving shape deformation. On the other hand, as far as numerics is concerned, we analyze a specific quantum-mechanical model defined by Eq. (2). The numerical model is motivated by the quarter stadium billiard system Hamiltonian, but still it is not literally the same model. In particular, Eq. (2) does not possess the semiclassical regime which has been discussed in the preceding section.

V. THE EVOLVING ENERGY DISTRIBUTION

In the case of the time independent Hamiltonian, the energy distribution does not change with time. In order to have an "evolving" energy distribution, we have to make $\delta x(t)$ time dependent. One possibility is to assume linear driving. In such a case, we write $\delta x(t) = Vt$. But more generally, for a cycle, we write $\delta x(t) = Af(t)$, with the convention $f(0) = f(T) = 0$. In some equations below, whenever a linear driving is concerned, A can be replaced by V, which assumes the particular choice $f(t) = t$. For practical purpose, given $f(t)$, it is convenient to associate with it the spectral function

$$\tilde{F}_t(\omega) = \left| \int_0^t \dot{f}(t') e^{i\omega t'} dt' \right|^2. \tag{3}$$

Some useful cases are summarized in Appendix A. In this paper, we are primarily interested in the case of triangular pulse [Eq. (A10)].

Given the model Hamiltonian [Eq. (2)], and the driving scheme $\delta x(t)$, we can calculate the unitary evolution operator $U(t)$. This kernel propagates "wave functions" in time. Equivalently, we can describe the quantum-mechanical state using a probability density matrix. The propagator of the latter is denoted by $\Lambda(t)$. In order to describe the evolution of the energy distribution, we define the kernel

$$P_t(n|m) = \text{tr}[\rho_n \Lambda(t) \rho_m]$$
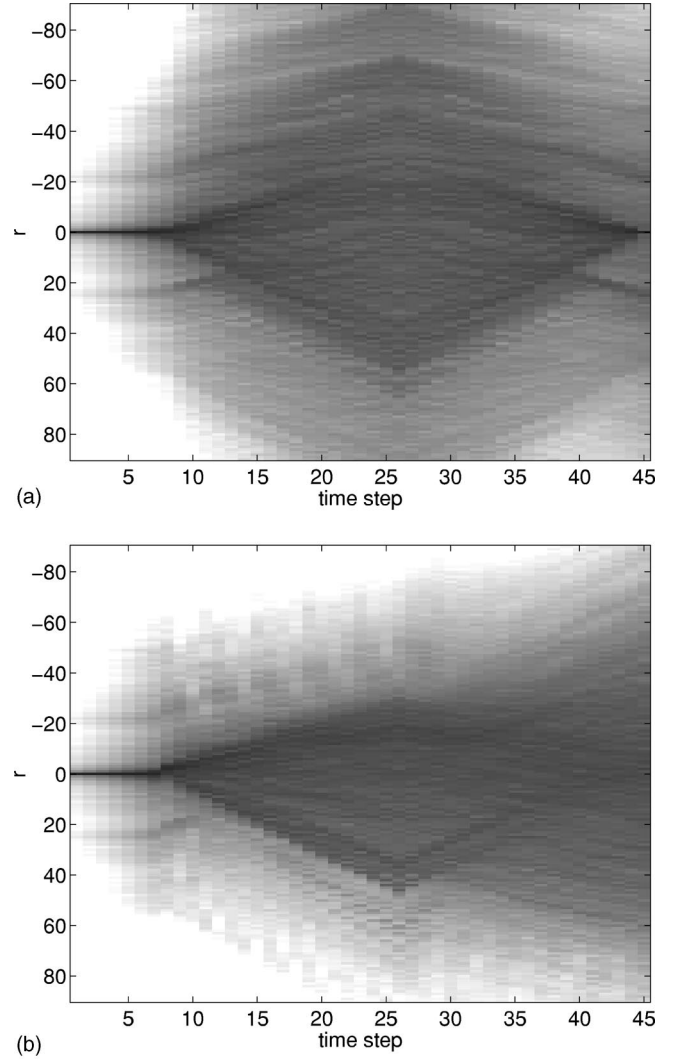$$= |\langle n(x(t))|U(t)|m(x(0))\rangle|^2, \tag{4}$$

FIG. 1. Images of time evolution within one-pulse period for $V = 100$ (upper panel) and for $V = 1$ (lower panel). Each column is a profile of the probability distribution $P_t(r)$ for a different time step t. The first seven time steps are log spaced, while the rest are linearly spaced. The $V = 100$ evolution is predominantly parametric.

where ρ_n can be interpreted as either the probability matrix or as the corresponding Wigner function that represents the eigenstate $|n\rangle$. In the latter case, the trace operation should be interpreted as $dPdQ/(2\pi\hbar)^d$ integration over phase space, where (Q,P) are the canonical coordinates of the particle, and $d = 2$ is the dimensionality.

We shall use the notation $P_t(r) = P_t(n-m) = P_t(n|m)$, with implicit average over the reference state m. We shall refer to $P_t(r)$ as the "average spreading profile." Whenever we have a wide distribution, we disregard the distinction between "energy difference" and "level difference," and make the identification

$$E_n - E_m \equiv \hbar\omega_{nm} \approx \Delta \times r, \tag{5}$$

where Δ is the mean-level spacing and $r = n - m$. (In our numerics $\Delta \approx 7.22$.)

Figure 1 displays the evolution as a function of time. Each
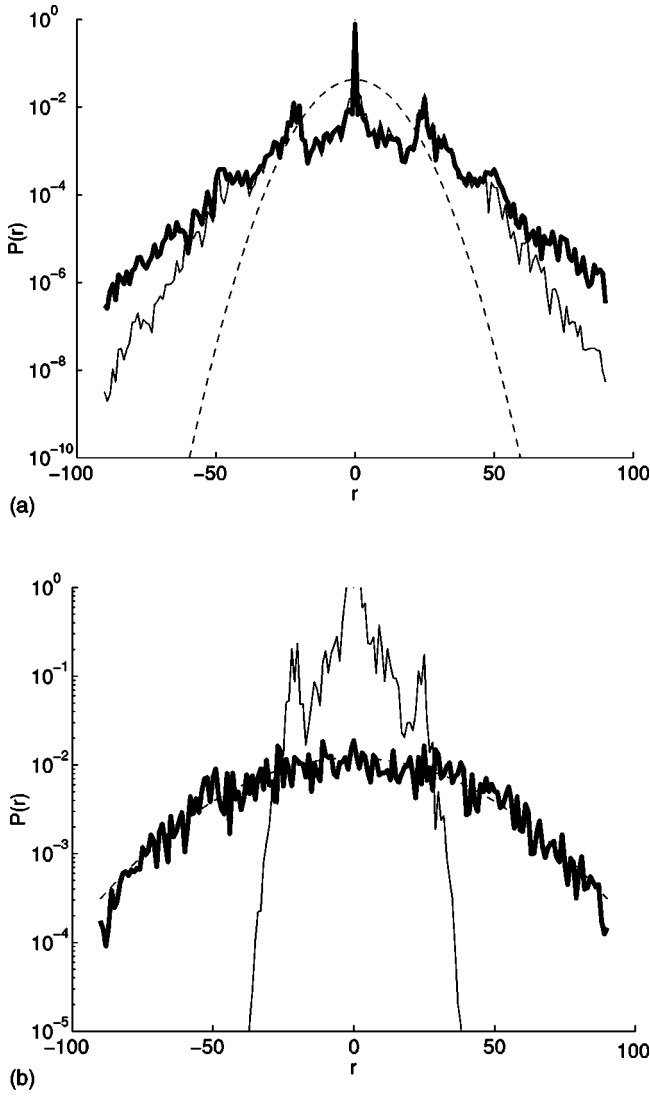
(a)

(b)

FIG. 2. Spreading profile at the end of one pulse period for $V = 100$ (upper panel) and for $V = 10$ (lower panel). The thin solid lines are from standard first-order perturbation theory, which means P_t^{prt} of Eq. (10) with $\Gamma = 0$. The dashed lines are for the Gaussian with the same variance.

column is a profile of the probability distribution $P_t(r)$. The first seven time steps are log spaced, while the rest are linearly spaced. The $V = 100$ evolution is predominantly parametric. As V becomes smaller and smaller, the deviation from parametric evolution becomes larger and larger. Some representative spreading profiles are presented in Fig. 2.

There are various practical possibilities available for the characterization of the distribution $P_t(r)$. It turns out that the major features of this distribution are captured by the following three measures:

$$\mathcal{P}(t) = P_t(r=0), \tag{6}$$

$$\Gamma(t) = 50\% \text{ probability width}, \tag{7}$$

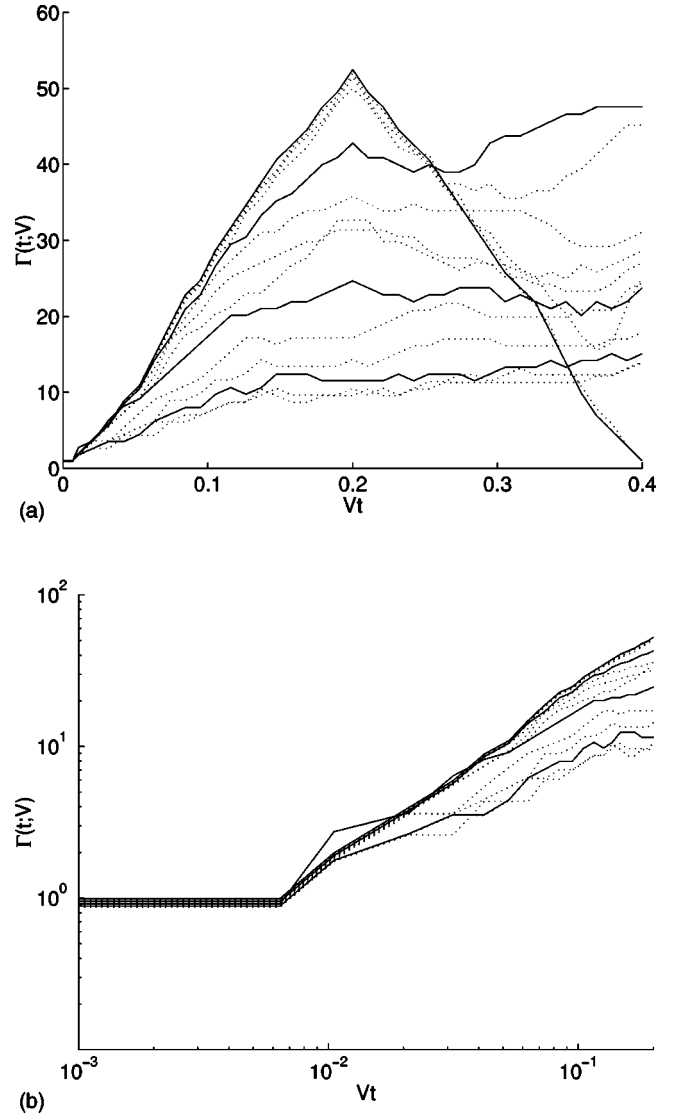$$\delta E(t) = \left(\sum_r r^2 P_t(r) \right)^{1/2} \Delta. \tag{8}$$

(a)

(b)

FIG. 3. The width $\Gamma(t)$ as a function of time. The numerical determination of Γ is explained after Eq. (7). The horizontal axis is the scaled time Vt. The different curves correspond to the different velocities $V = 100, 80, 40, 20, 10, 7, 5, 3, 1, 0.5, 0.2, 0.1, 0.07, 0.05$. The solid lines highlight the velocities $V = 100$ (uppermost), 10, 1, and 0.1. The lower panel is the same as in the upper figure, but in log-log scale, and only half period is displayed.

The first measure is the survival probability $\mathcal{P}(t)$. It is mentioned here just for completeness of presentation. The second measure $\Gamma(t)$ is the energy width of the central r region that contains 50% of the probability. It is calculated as $\Gamma(t) = (r_{75\%} - r_{25\%})\Delta$, where $r_{25\%}$ and $r_{75\%}$ are the values for which the cumulative energy distribution equals 25% and 75%, respectively. Finally, the energy spreading $\delta E(t)$ is defined above as the square root of the variance.

Figure 3 shows how the width $\Gamma(t)$ of the profile evolves. The lower panel of Fig. 3 is a log-log plot. We see clearly that up to $\delta x_c = 0.006$, the width is one level, which is an indication for the applicability of standard first-order perturbation theory. For larger δx, several levels are mixed nonperturbatively and, therefore, the width becomes larger than 1.
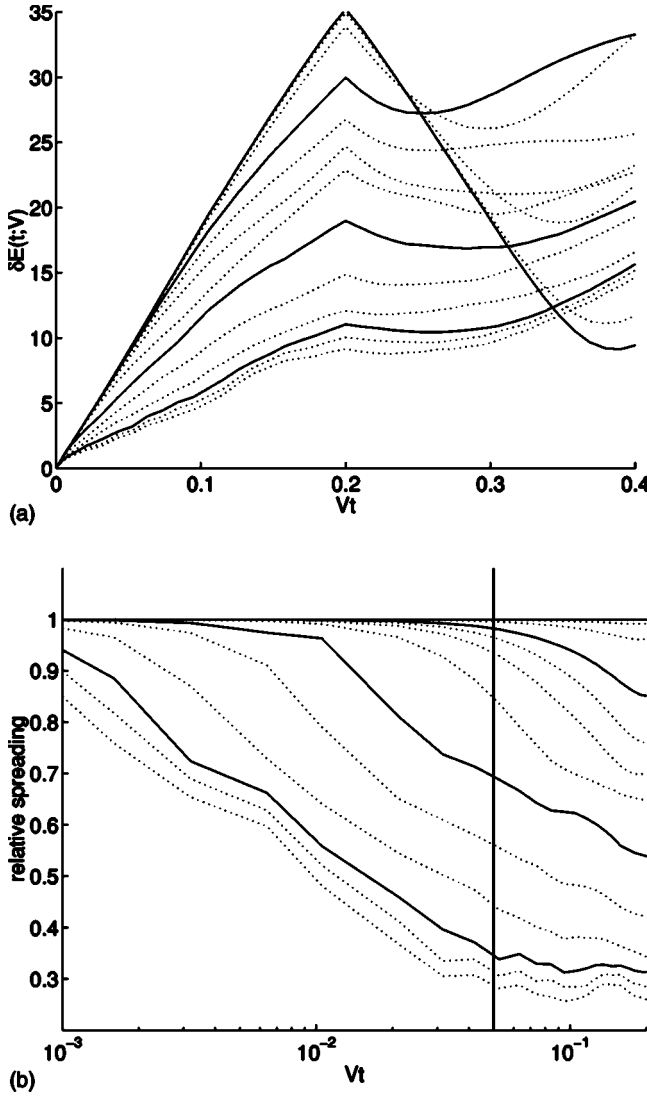
FIG. 4. The spreading $\delta E(t)$ of Eq. (8) as a function of time, for different V simulations. The upper panel is in one to one correspondence with the upper panel of the previous figure. In the lower panel, the data of the upper panel are presented in a different way: the vertical axis is the relative spreading, the horizontal axis is log scale, and only the half period is displayed. The location of δx_{prt} $= 0.05$ is indicated by vertical line. See the text for more details.

Figure 4 shows how the spreading $\delta E(t)$ of the profile evolves. The lower panel displays the relative spreading, which is defined as the ratio between the actual spreading and the parametric one. The notion of parametric evolution is defined in the next paragraph. As V becomes smaller, the departure from the parametric behavior happens earlier.

The sudden limit $(V \to \infty)$ of $P_t(n|m)$ will be denoted by $P(n|m)$. We shall refer to it as the parametric kernel. It is formally obtained by the replacement $\Lambda(t) \mapsto 1$, or equivalently $U(t) \mapsto 1$ in Eq. (4), namely,

$$P(n|m) = \text{tr}(\rho_n \rho_m)$$
$$= |\langle n(x(t))|m(x(0))\rangle|^2. \tag{9}$$

Obviously, its dependence on t is exclusively via $\delta x = x(t) - x(0)$, irrespective of V. The parametric evolution of $P(r)$ versus δx for a deforming billiard has been studied in Ref. [13]. The numerics in this paper can be regarded as an extension of the numerics of Ref. [13] to the case of finite V.

VI. THREE-PHASE STRATEGY

In the future we want to have a theory that allows the prediction of the (numerically simulated) time evolution. The minimum input that is required for such theory is the band profile of the **F** matrix. For precise definition of the band profile, see Appendix B. Note the existence of a very efficient semiclassical recipe to find the band profile. This can save the need for tedious quantum-mechanical calculations.

Using the band profile, one hopes to be able, in the "second phase" [20], to calculate the parametric kernel $P(n|m)$. The band profile does not contain information about the correlations between the off-diagonal elements. Therefore, one has to make the so-called random matrix theory (RMT) conjecture, namely, to assume that the off-diagonal elements are effectively uncorrelated. It turns out that, upon using such conjecture, the nonuniversal features of the parametric evolution are lost. Still, the obtained results are qualitatively correct and, therefore, such an approach is legitimate as an approximation.

However, finding the parametric kernel $P(n|m)$, using the band profile as an input, is not the subject of this paper. Therefore, as a matter of strategy, we would like to take the numerically determined parametric evolution as an input. Given the parametric kernel $P(n|m)$, the question is whether we can calculate the actual evolution $P_t(n|m)$ for any finite V.

In previous works (see review in Ref. [2]), we gave a negative answer to the above question. We have claimed that nonperturbative features of the dynamics cannot be deduced from the parametric analysis. To explain this observation, let us assume that we have two model Hamiltonians, say $\mathcal{H}_{physical}(x)$ and $\mathcal{H}_{artificial}(x)$. Let us assume further that the two models have the same band profile and the same parametric kernel $P(n|m)$. Still we claim that for finite V, the two Hamiltonians may generate *different* temporal kernels $P_t(n|m)$. In particular, it has been argued that this is in fact the case if $\mathcal{H}_{artificial}(x)$ is an effective RMT model which is associated with $\mathcal{H}_{physical}(x)$.

In past publications, the manifestation of nonperturbative features in case of driven physical (non-RMT) models has not been investigated numerically. On the theoretical side, it is an open subject for further research [15]. The purpose of the following sections is to present a strategy for analysis of numerical simulations that paves the way towards a theory for the nonperturbative aspects of the energy spreading.

VII. THE BAND PROFILE

The band profile of **F** is described by the spectral function $\tilde{C}(\omega)$, which is a Fourier transform of a correlation function $C(\tau)$. See Appendix B. If the collisions are uncorrelated, as in the case where the deformation involves only a small sur-
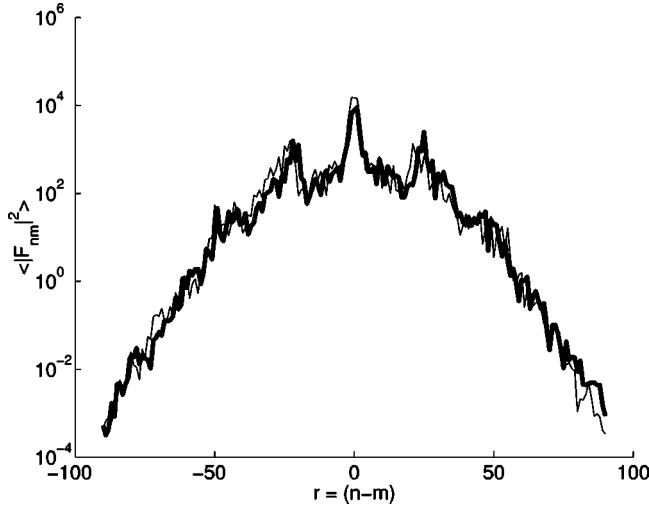
FIG. 5. The band profile, as defined in Appendix B. The two curves are the outcome of two different numerical procedures: the thin line is based on direct evaluation of matrix elements, while the thick line is deduced from the evolution over an infinitesimal time step (see Sec. XII for further details). A third possible procedure (not displayed) is to use the semiclassical recipe, Eq. (B3).

face element, then $C(\tau)$ is a δ function, and the band profile is flat. This is not the case in the present model. The correlations between collisions cannot be neglected and, therefore, $C(\tau)$ equals δ function plus a smooth component [18]. Due to the smooth component, the band profile has a very pronounced nonuniversal structure. See Fig. 5.

For large enough ω, the contribution of the nonuniversal component vanishes. Thus, the band profile should possess flat tails. These tails reflect the presence of the δ-function component in $C(\tau)$. For numerical reasons, due to truncation, the band profile of our system is multiplied by a Gaussian envelope. Therefore, the tails of the effective band profile are not flat, but rather vanishingly small. The lack of flat tails in the numerical model can be loosely interpreted as having "soft" rather than "hard" walls.

Thus, our system is characterized by a finite bandwidth. This is actually the generic case. Namely, for generic ("smooth") Hamiltonian, the correlation function $C(\tau)$ is nonsingular, which implies finite bandwidth.

VIII. APPROXIMATIONS

A major issue in the studies of energy spreading is the knowledge of how to combine tools or approximations in order to understand or calculate the kernel $P_t(n|m)$. In particular, we have the following approximations:

(1) The perturbative kernel $P_t^{\mathrm{prt}}(n|m)$.
(2) The semiclassical kernel $P_t^{\mathrm{scl}}(n|m)$.
(3) The Gaussian kernel $P_t^{\mathrm{sto}}(n|m)$.
(4) The parametric kernel $P(n|m)$.

The parametric kernel $P(n|m)$ that corresponds to the sudden limit ($V \rightarrow \infty$) has already been defined in Eq. (9). The other kernels will be defined in the present section. Obvi-

ously, the kernels listed above are very different. Our aim is to clarify in what regime (V), in what time stage (t), and in what energy region (r), which of them is the valid approximation.

The semiclassical kernel $P_t^{\mathrm{scl}}(n|m)$ is defined and obtained by assuming in Eq. (4), that the Wigner functions can be approximated by smeared microcanonical distributions. See Refs. [17,13,20] for further details and numerical examples. Whenever $P_t(n|m) \sim P_t^{\mathrm{scl}}(n|m)$, we say that the spreading profile is "semiclassical." In order to have a valid semiclassical approximation in case of billiard systems, the displacement δx of the walls should be much larger than the de Broglie wavelength [13]. Thus, for reasons that were explained in Sec. III, the semiclassical approximation is not applicable for the numerical model that we consider in this paper.

The perturbative kernel $P_t^{\mathrm{prt}}(n|m)$ is obtained from perturbation theory [17,16]. The defining expression is

$$P_t^{\mathrm{prt}}(n|m) = A^2 \widetilde{F}_t\left(\frac{E_n - E_m}{\hbar}\right)$$

$$\times \frac{\Delta}{2\pi\hbar}\widetilde{C}\left(\frac{E_n - E_m}{\hbar}\right) \frac{1}{\Gamma^2 + (E_n - E_m)^2},$$

(10)

where Γ is determined by *normalization*. If we make the replacement $\Gamma \mapsto 0$, we get the standard result of first-order perturbation theory [see Eq. (D5)]. The presence of Γ in the denominator reflects corrections to infinite order. We note that $P_t^{\mathrm{prt}}(n|m)$ constitutes a generalization of Wigner Lorentzian. We indeed would get from it a Lorentzian if the band profile were flat with no finite bandwidth.

Whenever $P_t(n|m) \sim P_t^{\mathrm{prt}}(n|m)$, we say that the spreading profile is "perturbative." The perturbative structure is characterized by having separation of scales

$$\Gamma(t) \ll \delta E(t). \quad (11)$$

We say that $P_t(n|m)$ has a "standard" perturbative structure [Eq. (D5)], which is given by first-order perturbation theory, if $\Gamma < \Delta$. This means that more than 50% probability is concentrated in the initial level. We use the term "core-tail" structure if we want to emphasize the existence of a finite nonperturbative core region $|r| < \Gamma/\Delta$. The core width Γ, as determined by perturbation theory by imposing normalization on Eq. (10), constitutes a rough estimate for the width $\Gamma(t)$ of the energy distribution [Eq. (7)].

The spreading $\delta E(t)$ for the core-tail structure is determined by the tail region, which is defined as $|r| \gg \Gamma/\Delta$. If Eq. (10) were a Lorentzian, it would imply $\delta E(t) = \infty$. This is of course not the case because the spectral functions provide a physical cutoff. Thus, the core-tail structure which is described by Eq. (10) is characterized by a tail component that contains a vanishingly small probability but still dominates the variance.

If we do not have the separation of energy scales Eq. (11), then perturbation theory becomes useless [17,16]. In such a

case, $P_t(n|m)$ becomes purely nonperturbative. In order to determine $P_t(n|m)$, we have to use tools that go beyond perturbation theory. In particular, for long times, one can justify [17,16] a stochastic approximation leading to the Gaussian kernel

$$P_t^{\text{sto}}(n|m) = \frac{1}{\sqrt{2\pi}} \frac{\Delta}{\delta(E(t))} \exp\left[-\frac{1}{2} \left(\frac{E_n - E_m}{\delta(E(t))} \right)^2 \right]. \quad (12)$$

Note that for very long times, this Gaussian should be replaced by an appropriate solution of a diffusion equation. But this is not relevant to our simulations. For a critical discussion that incorporates estimates for the relevant time scales, see Refs. [17,16].

A final remark is that for a Gaussian profile, the 50% width is $\Gamma(t) = 1.35 \, \delta E(t)$. However, whenever a nonperturbative structure is concerned, it is better, in order to avoid confusion, not to use the notation $\Gamma(t)$. The notation Γ has been adopted in the common diagrammatic formulation of the perturbation theory. In case of nonperturbative structure, this formulation becomes useless and, therefore, the significance of Γ, as a distinct energy scale, is lost.

IX. ANALYSIS OF THE PARAMETRIC EVOLUTION, δx REGIMES

The parametric evolution of $P(n|m)$ is illustrated in Fig. 1 (upper panel). For very small δx, we observe clearly a standard perturbative profile [Eq. (D5)], whose structure is just a reflection of the band profile. By definition, this holds in the standard perturbative (parametric) regime $\delta x < \delta x_c$. From the numerics (looking on the lower panel of either Fig. 3 or Fig. 6), we find that $\delta x_c = 0.006$.

For $\delta x > \delta x_c$, the initial level starts to mix with neighboring levels. As a result, a nonperturbative core component starts to develop. Thus, we obtain a core-tail structure. The tail is the perturbative component. The main component of the tail is the first-order tail which can be calculated using first-order perturbation theory. The tails in the vicinity of the core are growing slower, which can be regarded as a suppression of core-to-tail transitions due to the mixing. There are also higher-order tails [20] which can be neglected.

Having $\delta E \gg \Gamma$ is an indication that δE is dominated by the (perturbative) tail component of the core-tail structure Eq. (10). The condition $\Gamma \ll \delta E$ can be rewritten as $\delta x \ll \delta x_{\text{prt}}$, which constitutes a definition of the extended perturbative (parametric) regime. Unfortunately, the strong inequality $\Gamma \ll \delta E$ is nowhere satisfied in our numerics. Therefore, the numerical definition of δx_{prt} becomes ambiguous. One may naively define δx_{prt} by transforming the weak inequality $\Gamma < \delta E$ into a weak inequality $\delta x < \delta x_{\text{prt}}$. But this procedure is numerically meaningless: the quantities Γ and δE are energy scales. As such, their definition is arbitrary up to a prefactor of order unity. After some thinking, one realizes that the only practical definition for δx_{prt} is as the δx where the P_t^{prt} based prediction of δE becomes significantly less than the actual spreading. From the numerics (Fig. 6), we find that $\delta x_{\text{prt}} = 0.05$. This definition is not ambiguous numerically because we compare "variance based measure"
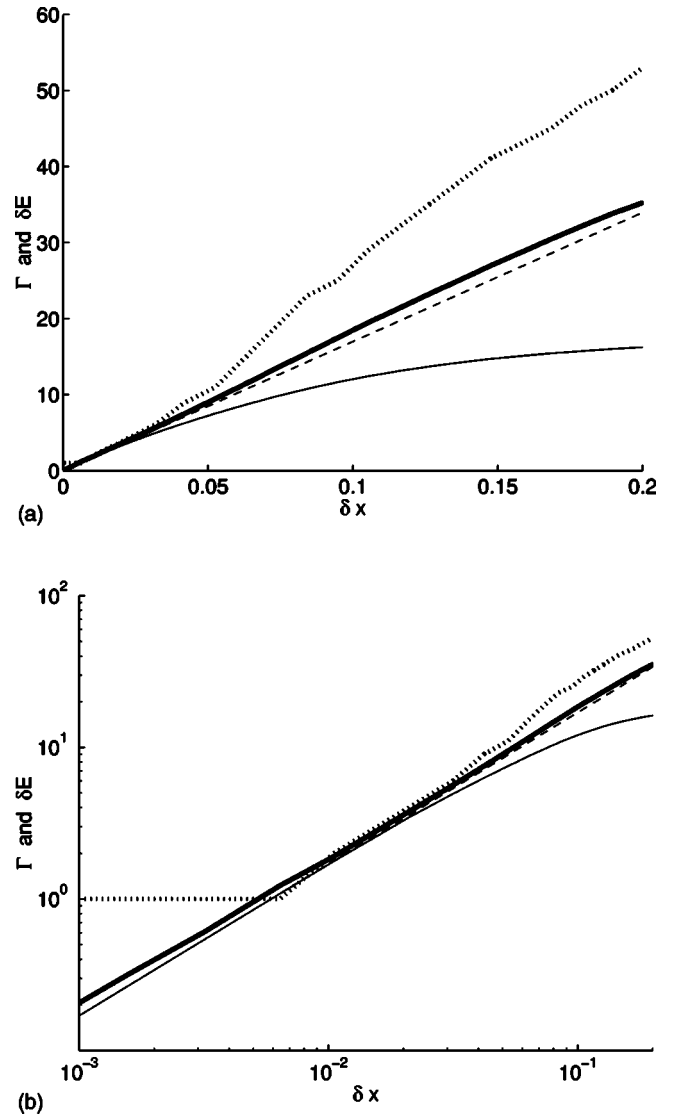

FIG. 6. Parametric evolution: the horizontal axis is δx either in linear scale (upper panel) or in logarithmic scale (lower panel). The dotted line is the width Γ from Eq. (7). The thick line is δE from Eq. (8), while the dashed line is the LRT estimate Eq. (16). The thin line is the perturbative estimate Eq. (8) using Eq. (10). From these plots, we can determine $\delta x_c = 0.006$ and $\delta x_{\text{prt}} = 0.05$.

(δE) to variance based measure (δE^{prt}), rather than comparing variance based measure (δE) to a "width measure" (Γ).

For $\delta x \gg \delta x_{\text{prt}}$, the P_t^{prt} based calculation of δE gives saturation. This (nonphysical) saturation is the consequence of having a finite bandwidth. It should be regarded as an artifact that reflects the limited validity of perturbation theory.

In the nonperturbative (parametric) regime, namely, for $\delta x > \delta x_{\text{prt}}$, the tails are no longer the dominant component. This is associated with a structural change in the spreading profile. Looking at the upper panel of Fig. 1, we observe a core-tail structure up to the 13th time step. Then, the secondary lobe of the band profile is swallowed by the core. This happening is reflected in Fig. 6 (upper panel) by a boost in the width Γ. [The notion of secondary lobe should be clear

by looking at the $|r| \sim 20$ region in the upper panel of Fig. 2. Unfortunately, its visibility in the corresponding image (upper panel of Fig. 1) is quite poor. Still it is possible to follow the evolution of the $r \sim 20$ tail region, and to realize that it is swallowed by the core.]

To have a weak inequality, $\delta x > \delta x_{\mathrm{prt}}$ is not quite the same as to be in the (deep) nonperturbative regime where $\delta x \gg \delta x_{\mathrm{prt}}$. For $\delta x > \delta x_{\mathrm{prt}}$, we do not get a purely nonperturbative structure. In spite of the failure of the core-tail picture Eq. (10), we still can make a *phenomenological* distinction between core and tail regions. One clearly observes that the tail region is "pushed" outside because of the expanding core. This nonperturbative effect is not captured by Eq. (10). In a previous study [13], the crossover from a core-tail structure to a purely nonperturbative (semiclassical) structure was quite abrupt. In the present study, the "deep" nonperturbative regime, where all the tail components disappear, is not accessible due to numerical limitations. A purely nonperturbative structure would be obtained if all the tail components were swallowed by the expanding core.

X. ANALYSIS OF ACTUAL EVOLUTION, V REGIMES

We start this section with a qualitative description of the actual evolution, which is based on looking in illustrations such as in Figs. 1 and 2. Later, we present the quantitative analysis. In general, one observes that for finite V the evolution acquires stochasticlike features. At intermediate times $(0 < t < T)$, the spreading profile contains both parametric and stochastic components. The parametric component is reversible. In contrast to that, the stochastic component of the spreading is not affected by the velocity reversal, and may lead to a final Gaussian distribution.

Let us describe what happens to the evolution, as a function of $\delta x = Vt$, as we make simulations with smaller and smaller V. On the basis of Eq. (10), we expect to observe a modulation of the tails of $P_t(r)$ in a way that is implied by the presence of envelope $\tilde{F}_t(\omega)$. This modulation is characterized by the energy scale $\hbar/t = \hbar V/\delta x$. If we make V further and further smaller, the secondary lobes of the tails [see preceding section for definition] do not have a chance to become visible because they are suppressed by the narrower envelope $\tilde{F}_t(\omega)$. For small enough V, only the main core component of the band profile is left visible. For very small V, the spreading profile becomes very close to a Gaussian shape in a very early stage of the evolution.

The spreading at the end of the pulse period is very small both in the sudden limit (very large V, corresponding to multiperiod driving with large frequency), and also in the adiabatic limit (very small V). Figure 2 illustrates representative spreading profiles, which are observed in the end of the pulse period. Also displayed are the first-order perturbative profile [Eq. (D5)] and a Gaussian with the same width. Note that the first-order perturbative profile Eq. (D5), unlike Eq. (10), does not have a proper normalization. We can define a "difference measure" in order to quantify the deviation of the (actual) line shape from Gaussian shape. One possible definition is

$$\sqrt{\sum_r P^{\mathrm{sto}}(r)\{\log[P_t(r)] - \log[P_t^{\mathrm{sto}}(r)]\}^2}. \quad (13)$$

The lower panel of Fig. 8 shows that for $V < 20$, the spreading profile at the end of the pulse is close to Gaussian shape, while for $V > 20$ this profile is predominantly of perturbative nature.

We should address now the issue of V regimes. Namely, for a given V, we would like to characterize the nature of the dynamical scenario. Below, we shall introduce a practical procedure for the identification of the various regimes. We are going to explain that in the numerical simulation, we observe following four different V regimes:

(1) Adiabatic regime ($V < 3$).
(2) Perturbative regime ($3 < V < 7$).
(3) Nonperturbative regime ($7 < V < 20$).
(4) Sudden regime ($20 < V$).

Before we get into details, we would like to make a connection with the theoretical discussion of regimes in Ref. [15]. There we have considered a (sinusoidal) periodic driving that is characterized by amplitude A and frequency $\Omega = 2\pi/T$. For sinusoidal driving, the root-mean-square "velocity" is $V = A\Omega/\sqrt{2}$. So fixing A and changing V in the present paper, is completely analogous to fixing A and changing Ω in Ref. [15]. Thus, the four V regimes listed above correspond to a horizontal cut ($A = \mathrm{const} > A_{\mathrm{prt}}$) in the (Ω, A) regime diagram of Ref. [15] (see Fig. 1 there). One should realize that the perturbative regime is in fact the linear response (Kubo) regime as defined in Ref. [15], and that the sudden regime corresponds to the regime of vanishing (high frequency) response.

In the adiabatic V regime, the spreading is due to near-neighbor level transitions, and disregarding extremely short times (for which we can apply standard first-order perturbation theory [Eq. (D5)], it looks stochastic. This means that Eq. (12) is a quite satisfying approximation. For further details regarding the identification of the adiabatic regime, see Sec. XII.

Outside the adiabatic regime, there is a time stage where perturbation theory [Eq. (10)] is valid. But after this time, we have to use theoretical considerations that go beyond perturbation theory. In the following paragraph, we divide the nonadiabatic regime into perturbative V regime, nonperturbative V regime, and sudden regime. The basis for this distinction is the timing of the *departure* from parametric evolution. The departure from parametric evolution is best illustrated by the lower panel of Fig. 4.

The perturbative V regime is defined by the requirement of having the *departure* from parametric evolution happen *before* the breakdown of Eq. (10). Consequently, in this regime, the departure time can be deduced from Eq. (10). For example, let us assume a simple band profile. In such a case, departure time is just the inverse of the bandwidth, which implies via Eq. (B3) that it is simply the classical correlation time τ_{cl} of the chaotic motion. In the actual numerical analysis, the band profile is not simple, but has some structure. Rather than debating over the definition of τ_{cl}, it is more

practical to determine the departure time by inspection of Fig. 4. For convenience, we have indicated the location of δx_{prt} by a vertical line. For $V<7$, the departure from parametric evolution happens before this line. This way one can determine the upper border ($V=7$) of the perturbative regime.

The nonperturbative V regime is defined by the requirement of having the *departure* from parametric evolution happen *after* the breakdown of Eq. (10). In other words, it means that this departure cannot be captured by perturbation theory. A more careful definition of the nonperturbative regime should take into account the driving reversal at $t=T/2$. As explained in the next paragraph, the nonperturbative regime is further restricted by the requirement of having the *departure* from parametric evolution happen *before* the driving reversal.

The distinction between perturbative and nonperturbative V regimes is related to the possibility to capture the *stochastic* features of the energy spreading by perturbation theory. Nonperturbative features of the energy distribution during intermediate times are of no relevance if they are of parametric (nonstochastic) origin. Let us see, for example, the upper panel of Fig. 1. We clearly see that the spreading profile at the end of the pulse (at $t=T$) is of a standard perturbative nature. All the nonperturbative features that develop during the first half of the driving cycle are completely reversed in the second half of the cycle.

Conceptually, the simplest way to set a criterion for getting to the end of the pulse, a perturbative structure is to use fixed basis perturbation theory (see Appendix C of Ref. [16]). If we adhere to the present (more physical) approach of using x-dependent basis, an equivalent method [16] is to determine the sudden time t_{sdn}. This is the time to resolve the expanding core. It is determined as the time when the following inequality is violated:

$$\Gamma(t)\ll\hbar/t. \qquad (14)$$

The regime, where the condition $t_{\mathrm{sdn}}\ll T$ is violated, is defined as the sudden regime. In the sudden regime, all the nonperturbative features are of parametric nature, and therefore the validity of perturbation theory survives at the end of the pulse. In the sudden regime, the *departure* from parametric evolution becomes visible only *after* the driving reversal. One can determine the sudden regime simply by looking at the lower panel of Fig. 8. The departure of the energy distribution (at $t=T$) from Gaussian shape is correlated with getting into the sudden regime.

The discussion above of V regimes was based on looking for the *breaktime* of perturbation theory [Eq. (10)], on one hand, and looking for the *departure* from parametric behavior on the other hand. The departure from parametric behavior is an indication for the appearance of a predominant stochastic component in the spreading profile. This departure does not imply that we get a Gaussian line shape. In the perturbative regime, we get the Gaussian line shape *after* the breaktime of perturbation theory, which happens *after* the departure from parametric behavior. Therefore, in the perturbative regime, there are three stages in the evolution: a para-

metric stage, a perturbative stochastic stage, and a genuine stochastic stage. In contrast to that, in the nonperturbative regime, we do not have an intermediate perturbative stochastic stage because the departure from parametric behavior happens *after* the breakdown of perturbation theory.

XI. LRT FORMULA

The general LRT formula for the variance of the spreading is

$$\delta E(t)^2=A^2\int_{-\infty}^{\infty}\frac{d\omega}{2\pi}\widetilde{F}_t(\omega)\widetilde{C}(\omega). \qquad (15)$$

The proportionality $\delta E\propto A$ reflects having a linear response. Two spectral functions are involved: One is the the spectral content of the driving (Appendix A), and the other is the power spectrum of the fluctuations (Appendix B). The latter is the Fourier transform of a correlation function $C(\tau)$.

A special case is the sudden limit ($V=\infty$), for which $\widetilde{F}_t(\omega)=1$ and accordingly

$$\delta E(t)=\sqrt{C(\tau=0)}A. \qquad (16)$$

Another special case is the response for persistent (either linear or periodic) driving, where $\widetilde{F}_t(\omega)=t2\pi\delta(\omega)$ implies diffusive behavior:

$$\delta E=\sqrt{2D_Et}. \qquad (17)$$

In such a case, the expression for D_E is known as Kubo formula, leading to a fluctuation-dissipation relation.

Finding the conditions for validity of LRT is of major importance. This should be regarded as an important step in the analysis of the response of a driven system. The classical derivation of Eq. (15) is quite simple, and for completeness we present it in Appendix C. For the sake of the following discussion, one can assume that the classical "slowness" conditions for the validity of classical LRT are satisfied.

The quantum-mechanical derivation of this formula is much more subtle [17,14–16] and leads to the distinction between adiabatic, and (extended) perturbative and nonperturbative regimes. The semiclassical limit is contained in the latter regime. It is known that the LRT formula does not hold in the adiabatic regime [21], but it is valid in the (extended) perturbative regime [14,16]. It is not necessarily valid in the nonperturbative regime [14,15], but if the system has a classical limit, it must be valid again in the semiclassical regime. See further discussion in the following sections.

XII. ANALYSIS: COMPARISON WITH LRT

Using the band profile as an input, we can calculate the spreading using Eq. (15). In Fig. 6, the calculation is done for the parametric evolution [dashed line given by Eq. (16)], while in Fig. 7, the calculation is done with Eq. (15) for finite V values. The latter figure should be compared with the upper panel of Fig. 4. The agreement is very good unless the velocity V is small. See later discussion of the quantum-mechanical (QM)–adiabatic regime. The spreading δE at the
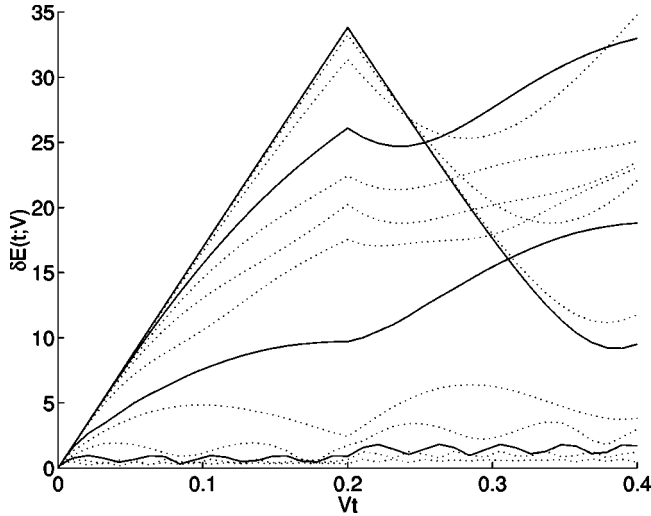
FIG. 7. LRT calculation of the spreading versus time, using Eq. (15) with the band profile as an input. The horizontal axis is Vt. This figure is in one to one correspondence with the upper panel of Fig. 4. One observes that for small V, the calculation underestimates the observed spreading. See discussion in Sec. XII.

end of the pulse is better illustrated in Fig. 8.

There are three possible strategies for evaluating the band profile. The first is to use the semiclassical strategy with Eq. (B3). The second is to make a careful numerical evaluation of the matrix elements, and to use the definition Eq. (B1). This gives the thin line in Fig. 5. However, the most practical and economical procedure is simply to deduce the band profile from the spreading profile $P(r)$ that corresponds to the smallest δx value. This is the thick line in Fig. 5, which we regard as the most appropriate estimate.

We found out that the LRT formula [Eq. (15)] is *not* sensitive to the way in which the band profile is evaluated, unless the $|n-m|=1$ elements of the $\mathbf{F}_{nm}$ matrix dominate the result. Let us denote by σ the root-mean-square magnitude of these matrix elements. The sensitivity to σ happens in the V regime, which is determined by the condition $V < (\Delta)^2/(\hbar\sigma)$, which is the adiabaticity condition. This sensitivity can be used as a practical tool for the determination of the adiabatic regime. In the upper panel of Fig. 8, we display the result of the LRT calculation upon setting $\sigma = 0$. We see that the LRT calculation implies QM-adiabatic behavior for $V < 3$.

If V is well away from the adiabatic regime, then near-neighbor level transitions have negligible contribution. In such a case, the LRT calculation is not sensitive to the exact value of σ. As V becomes smaller, there is a larger relative weight to the near-neighbor matrix elements.

Deep in the QM-adiabatic regime, the mean-level energy difference is resolved much *before* the levels are mixed, and therefore, as a result of recurrences, the probability stays concentrated in the initial level. This is, of course, a leading order description. In fact, we cannot neglect higher-order corrections.

In the adiabatic regime, the spreading is dominated by transition between neighboring levels (whereas outside of the adiabatic regime, the contribution of neighboring level tran-
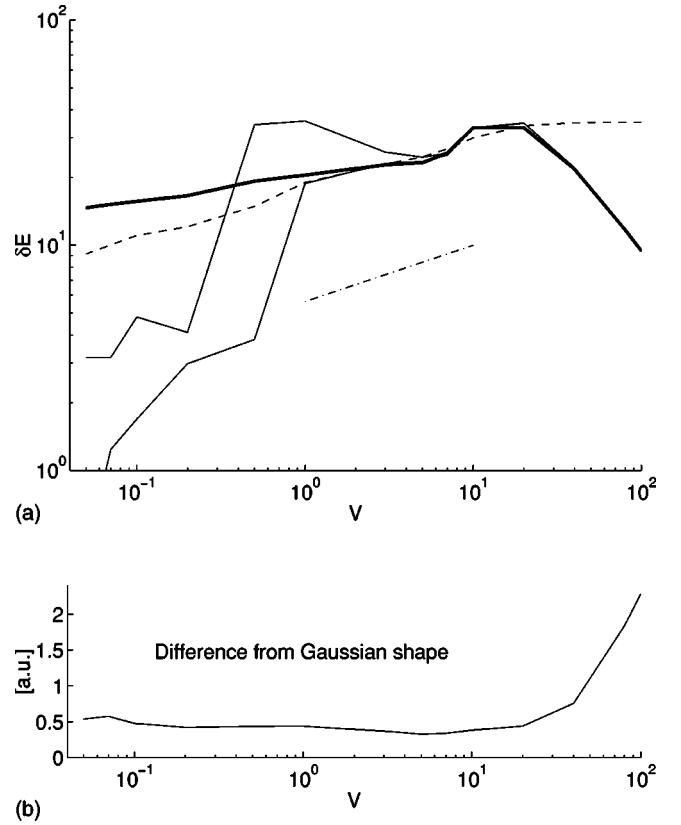

FIG. 8. Upper panel: response for one-pulse versus V. The thick line is δE at the end of the pulse. The thin (solid and dotted) lines correspond to the LRT calculation Eq. (15). For the calculation of the lower thin lines, we have set the near-level coupling $\sigma = 0$. The dashed line is the spreading at the end of half pulse period. The dash-dot line is the slope that corresponds to the Landau-Zener spreading mechanism. The lower panel is the difference Eq. (13) from Gaussian line shape.

sitions can be neglected). Therefore, it is only in the adiabatic regime, where the quantum-mechanical calculation [using Eq. (15)] gives results that are different from the classical expectation [22]. Is it possible to witness a regime where the quantum-mechanical (rather than the classical) LRT prediction is observed? Apparently, the answer is positive, but not in a typical numerical experiment. The reason is that almost always the Landau-Zener (non-LRT) mechanism for energy spreading takes over [21].

We can verify the dominance of Landau-Zener mechanism as follows. The theoretical prediction is $\delta E(t) \propto \sqrt{D_E t}$ with $D_E \propto V^{3/2}$. In the upper panel of Fig. 8, we plot the spreading at the end of half pulse period ($t = T/2 = A/V$) and at the end of full pulse period ($t = T = 2A/V$). Hence, we expect $\delta E \propto V^{1/4}$. The agreement with this expectation is quite good if we consider the spreading after half pulse period. At the end of full pulse period, we see that the spreading is larger than expected. This is apparently due to the nonadiabatic nature of the $V \mapsto -V$ switching.

XIII. DISCUSSION AND CONCLUSIONS

The numerical study that we have presented should be regarded as an application of a general procedure for the

analysis of energy spreading. In the summary below, we re-order the stages in this analysis in the way which is implied by the results of the earlier sections.

The first step in the analysis is to find the band profile. This can be done using the semiclassical recipe (Appendix B) without any need to make heavy numerical simulations. Then it is possible to determine $\delta E(t)$ by using the LRT formula [Eq. (15)].

The second step in the analysis is to determine the adiabatic V regime. This is done by checking whether the LRT calculation of $\delta E(t)$ is sensitive to σ. In order to get in the adiabatic regime LRT-based quantum corrections to the classical result, we have to take the level spacing statistics into account [22,23]. We have pointed out the difficulty in observing such corrections. Rather we can improve over the LRT prediction by taking into account either higher-order or Landau-Zener corrections to perturbation theory.

The third step in the analysis is to calculate the parametric perturbative profile $P^{\mathrm{prt}}(r)$. This is associated with getting a rough *estimate* for the core width Γ. Also the parametric scales δx_c and δx_{prt} can be determined on the basis of this analysis. The former is determined from inspecting Γ, while the latter is determined by comparing δE of the LRT calculation to the P^{prt} based prediction.

The fourth step in the analysis is to distinguish between the perturbative and the nonperturbative regime. For this purpose, we have to look for the timing of departure from parametric behavior, as in the lower panel of Fig. 4. For δE, one can use the LRT based calculation of Eq. (15).

The fifth step in the analysis is to identify the sudden regime. For this purpose, we have to eliminate the sudden time from Eq. (14). The problem is to estimate $\Gamma(t)$ in the nonperturbative regime. If we have only the band profile as an input, then we can use the rough estimate $\Gamma(t) \sim \delta E(t)$. This is based on the assumption that in the nonperturbative regime, the energy distribution is characterized by a single energy scale.

The sixth step in the analysis is to make a simulation of the parametric evolution. This is a relatively heavy task, but it is still much easier than making finite V simulation. (It requires merely diagonalizations, while a temporal simulation requires an iterative procedure.) The main nontrivial effects that we have found in the analysis of the parametric evolution were the following:

(i) Higher-order tails grow up.
(ii) A non-perturbative core region develops.
(iii) The core-to-tail transitions are suppressed.
(iv) The tails are "pushed out."
(v) Tail components are swallowed by the expanding core.

The last two items are in the spirit of the core-tail theory, but go beyond the perturbative approximation [Eq. (10)]. Knowledge of the parametric evolution allows accurate determination of Γ, leading to a refined determination of the V regimes.

The seventh step in the analysis is to make simulation of the actual evolution. We would like to emphasize that here the different dynamical scenarios (corresponding to the dif-ferent V regimes) are illustrated in a numerical simulation. The only other numerical studies (mainly Refs. [15,12]) were too restricted in scope, and did not contain analysis of the stages in the evolution of the energy *distribution*.

The only nonperturbative effect on the response that we have discussed so far is the Landau-Zener correction to the spreading in the adiabatic regime. Are there any other nonperturbative effects that affect the response? The immediate tendency is to regard LRT as the outcome of standard first-order perturbation theory (Appendix D). Then the question that arises is what happens if Eq. (D5) does not apply?

Let us recall the answer in case of the parametric evolution of $P(n|m)$. As δx becomes larger, we should be worried regarding the implications of having the effects that are listed at the end of Sec. IX. Having expanding core that pushes out the tails, and having growing higher-order tail components, may suggest that the first-order calculation of the variance [Eq. (D7)] should be "corrected," and should include higher-order terms. Does it mean that Eq. (16) underestimates the spreading? Or maybe we should assume that Eq. (10) provides the correct "trend" of higher-order corrections? The tails in the vicinity of the core are growing slower, which can be regarded as a suppression of core-to-tail transitions due to the mixing. Consequently, we would conclude that Eq. (16) is an overestimation of spreading. Moreover, if we take Eq. (10) too seriously, beyond its regime of validity, we would conclude that the spreading has saturation for large δx.

For the parametric evolution, these possible speculations turn out to be *wrong*. The above effects are exactly balanced and the LRT formula [Eq. (16)] remains exact beyond any order of perturbation theory, which means that it is exact even in the nonperturbative regime where perturbation theory is not applicable. This claim has a simple derivation [20]. Note also that if the system has a classical limit, then the validity of Eq. (16) can be established deep in the nonperturbative regime, where the semiclassical approximation becomes reliable.

The question is whether this delicate balance is violated in case of finite V. For example, it may be that due to incomplete core-tail recurrences, we shall have enhanced spreading (compared with LRT). Unlike the parametric case, we do not have a theoretical proof that excludes such a possibility. In fact, contrary is the case. We have demonstrated that for an artificial (random matrix theory) model, the LRT formula *cannot be trusted* in the nonperturbative regime. Whether such an effect is possible also for a "quantized" system that possesses a good classical limit has been left an open question.

The possibility of having deviation from LRT in the nonperturbative regime was one important motivation for the present research. Clearly, we did not witness such an effect in our simulations (Fig. 8). This reflects that there is a clash between the semiclassical limit and the RMT limit.

ACKNOWLEDGMENTS

APPENDIX A: THE SPECTRAL FUNCTION $\tilde{F}_T(\omega)$

Given a function $f(t')$ that describes the shape of the driving pulse during the time interval $0 < t' < t$, we define a spectral function $\tilde{F}_t(\omega)$ by Eq. (3). This spectral function describes the spectral content of the driving pulse. Below we list some useful driving schemes. We use the notation $\Theta()$, which is defined by $\Theta(\text{false}) = 0$ and $\Theta(\text{true}) = 1$.

For the step function, we have

$$f(t') = \Theta(0 < t'), \tag{A1}$$

$$\tilde{F}_t(\omega) = 1. \tag{A2}$$

For the rectangular pulse, we have

$$f(t') = \Theta(0 < t' < t), \tag{A3}$$

$$\tilde{F}_t(\omega) = |1 - e^{i\omega t}|^2. \tag{A4}$$

If it is followed by a negative pulse, we get

$$f(t') = \Theta(0 < t' < t) - \Theta\left(\frac{T}{2} < t' < t\right), \tag{A5}$$

$$\tilde{F}_t(\omega) = |1 - 2e^{i\omega(T/2)} + e^{i\omega t}|^2 \quad \text{for } t > \frac{T}{2}. \tag{A6}$$

For linear driving, we have

$$f(t') = t', \tag{A7}$$

$$\tilde{F}_t(\omega) = t^2[\text{sinc}(\tfrac{1}{2}\omega t)]^2, \tag{A8}$$

where $\text{sinc}(\cdots) = \sin(\cdots)/(\cdots)$. Note that for very large t, we have

$$\tilde{F}_t(\omega) \sim t 2\pi \delta(\omega). \tag{A9}$$

Finally, for the triangular pulse

$$f(t') = 2\frac{t'}{T}\Theta\left(0 < t' < \frac{T}{2}\right) + 2\left(1 - \frac{t'}{T}\right)\Theta\left(\frac{T}{2} < t' < T\right), \tag{A10}$$

we get

$$\tilde{F}_t(\omega) = \left[\frac{2}{T}\right]^2 t^2[\text{sinc}(\tfrac{1}{2}\omega t)]^2) \quad \text{for } 0 < t < \frac{T}{2},$$

$$\tilde{F}_t(\omega) = \left[\frac{2}{T}\right]^2 \left|\frac{1 - 2e^{i\omega(T/2)} + e^{i\omega t}}{\omega}\right|^2 \quad \text{for } \frac{T}{2} < t < T.$$

APPENDIX B: THE SPECTRAL FUNCTION $\tilde{C}(\omega)$

Let us denote by $\mathbf{F}_{mn}$ the matrix representation of some quantized observable $F(Q,P)$, in the basis which is deter-

mined by some quantized chaotic Hamiltonian $\mathcal{H}(Q,P)$. The band profile of $\mathbf{F}_{mn}$ is conveniently characterized by the spectral function

$$\tilde{C}(\omega) = \sum_{n(\neq m)} |\mathbf{F}_{nm}|^2 2\pi\delta\left(\omega - \frac{E_n - E_m}{\hbar}\right), \tag{B1}$$

with an implicit average over the reference state m. This is the power spectrum of the fluctuating quantity $\mathcal{F}(t)$, whose classical definition is $\mathcal{F}(t) = F(Q(t), P(t))$, with a corresponding quantum-mechanical definition within the Heisenberg picture. The power spectrum of a fluctuating quantity $\mathcal{F}(t)$ is defined as the Fourier transform of the corresponding correlation function $C(\tau)$.

Chaotic systems are characterized by fast decay of dynamical correlations. We assume a separation of time scales between the (short) classical correlation time, and the (long) quantum-mechanical Heisenberg time. Thus, for times during which we can ignore the recurrences, we expect the following quantum-classical correspondence:

$$C(\tau) \approx C^{\text{cl}}(\tau). \tag{B2}$$

This correspondence implies that the envelope of $\tilde{C}(\omega)$ is given by $\tilde{C}^{\text{cl}}(\omega)$, and the following semiclassical expression for the matrix elements follows [24]:

$$\langle |\mathbf{F}_{nm}|^2\rangle \approx \frac{\Delta}{2\pi\hbar}\tilde{C}^{\text{cl}}\left(\frac{E_n - E_m}{\hbar}\right). \tag{B3}$$

Taking into account the level spacing statistics, we deduce the following relation [22]:

$$\tilde{C}(\omega) \approx \hat{R}(\omega)\tilde{C}^{\text{cl}}(\omega), \tag{B4}$$

where $\hat{R}(\omega) \propto \langle \sum_n \delta(\omega - \omega_{nm})\rangle_m$ is the two-point correlation function of the energy spectrum (Fourier transform of the spectral form factor). This function behaves as $\hat{R}(\omega) \sim \omega^\beta$ for small ω, and as $\hat{R}(\omega) \sim 1$ for large ω. For the Gaussian unitary ensemble (GUE) $\beta = 2$, and there is a simple expression:

$$\hat{R}(\omega)|_{\text{GUE}} = 1 - [\text{sinc}(\pi\hbar\omega/\Delta)]^2. \tag{B5}$$

For the system that we consider in this paper it is appropriate to assume $\beta = 1$, corresponding to the Gaussian orthogonal ensemble (GOE).

APPENDIX C: CLASSICAL DERIVATION OF THE LRT FORMULA

Consider $\mathcal{H}(Q,P;x(t))$, and define the following time dependent quantities:

$$\mathcal{F}(t) = -\frac{\partial\mathcal{H}}{\partial x}(Q(t), P(t); x(t)), \tag{C1}$$

$$\mathcal{E}(t) = \mathcal{H}(Q(t), P(t); x(t)), \tag{C2}$$

$$\mathcal{E}'(t) = \mathcal{H}(Q(t), P(t); x(0)). \tag{C3}$$

Note that $\mathcal{E}(t)$ is the energy in the conventional sense, while $\mathcal{E}'(t)$ is the energy using a "fixed basis." We have the following relations:

$$\frac{d\mathcal{E}(t)}{dt} = \frac{\partial \mathcal{H}}{\partial t} = -\dot{x}(t)\mathcal{F}(t), \tag{C4}$$

$$\frac{d\mathcal{E}'(t)}{dt} = -[\mathcal{H}, \mathcal{H}_0] \approx \delta x(t)\dot{\mathcal{F}}(t). \tag{C5}$$

The latter approximated equality strictly holds if the perturbation $\mathcal{H} - \mathcal{H}_0$ is linear with respect to the perturbation parameter $\delta x = x - x_0$. From the equations above, it follows that

$$\mathcal{E}(t) - \mathcal{E}(0) = -\int_0^t \dot{x}(t')\mathcal{F}(t')dt', \tag{C6}$$

$$\mathcal{E}'(t) - \mathcal{E}'(0) \approx \int_0^t \delta x(t')\dot{\mathcal{F}}(t')dt'. \tag{C7}$$

Obviously, the two latter expressions coincide for a cycle $[x(t) = x(0)]$. Squaring Eq. (C6), and performing a microcanonical average over the (implicit) initial conditions $[Q(0), P(0)]$, one obtains

$$\delta E(t)^2 = A^2 \int_0^t \int_0^t \dot{f}(t')\dot{f}(t'') C(t' - t'') dt' dt''. \tag{C8}$$

This can be written as Eq. (15).

APPENDIX D: FIRST-ORDER PERTURBATION THEORY AND LRT

For convenience, we assume that the perturbation is linear in $\delta x = x - x_0$. In complete analogy with the classical analysis, we can work either using fixed basis, or else we can use the proper x-dependent basis (the so-called adiabatic representation). The respective matrix representations of the Hamiltonian are

$$\mathcal{H} \mapsto \mathbf{E} + \delta x(t)\mathbf{F}, \tag{D1}$$

$$\mathcal{H} \mapsto \mathbf{E} + \dot{x}(t)\mathbf{W}, \tag{D2}$$

where $\mathbf{E}$ is a diagonal matrix. Note that in the first equation, $\mathbf{E}$ and $\mathbf{F}$ are calculated for $x = x_0$, while in the second equation there is an implicit $x(t)$ dependence. The matrix elements of $\mathbf{F}$ are

$$\mathbf{F}_{nm} = \left\langle n \left| \frac{\partial \mathcal{H}}{\partial x} \right| m \right\rangle. \tag{D3}$$

The off-diagonal matrix elements of $\mathbf{W}$ are

$$\mathbf{W}_{nm} = \frac{\hbar}{i}\left\langle n \left| \frac{d}{dt} m \right\rangle = i\frac{\hbar}{E_n - E_m}\mathbf{F}_{nm}, \tag{D4}$$

and we use the "gauge" convention $\mathbf{W}_{nm} = 0$ for $n = m$. (Only one parameter is being changed and therefore Berry's phase is not an issue.) The derivation of Eq. (D2) is standard, and can be found in Sec. XI of Ref. [16].

Using first-order perturbation theory with Eq. (D2), we get

$$P_t(n|m) = \delta_{nm} + A^2 \tilde{F}_t\left(\frac{E_n - E_m}{\hbar}\right)\left|\frac{\mathbf{W}_{nm}}{\hbar}\right|^2. \tag{D5}$$

Note that for a cycle $[f(t) = f(0) = 0]$, the same result is obtained via first order perturbation theory with Eq. (D1). As a global approximation [Eq. (D5)] is valid only in the standard perturbative regime. In the extended perturbative regime, it is valid only for the first-order tail region (see Sec. VIII). The expression for the first-order tail region can be written in a concise way as

$$P_t(n|m) = A^2 \tilde{F}_t(\omega_{nm})\frac{\Delta}{2\pi\hbar}\tilde{C}(\omega_{nm})\left[\frac{1}{\hbar\omega_{nm}}\right]^2. \tag{D6}$$

The corresponding global approximation is given by Eq. (10).

Assuming that the variance is dominated by the first-order tail component, we get the LRT result

$$\delta E(t)^2 = \sum_n P_t(n|m)(E_n - E_m)^2$$

$$= A^2 \int_{-\infty}^{\infty} \frac{d\omega}{2\pi\hbar}\tilde{F}_t(\omega)\tilde{C}(\omega). \tag{D7}$$

An implicit average over m is assumed. Note that the latter formula does not contain $\hbar$. This restricted quantum-classical correspondence holds only for the variance. Higher moments of the energy distribution are typically much smaller compared with the classical expectation, and scale like $\hbar$ to the power of the moment order -2.

---

[1] For a pedagogical presentation, including references, see Refs. [2] and [17], which can be downloaded from http://www.bgu.ac.il/~dcohen

[2] D. Cohen, in *Dynamics of Dissipation*, Proceedings of the 38th Karpacz Winter School of Theoretical Physics, edited by P. Garbaczewski and R. Olkiewicz (Springer-Verlag, Berlin, 2002).

[3] S.W. Doescher and M.H. Rice, Am. J. Phys. **37**, 1246 (1969).

[4] A.J. Makowski and S.T. Dembinski, Phys. Lett. A **154**, 217 (1991).

[5] J.V. Jose and R. Cordery, Phys. Rev. Lett. **56**, 290 (1986).

[6] For review and references, see Refs. [8,9].

[7] E. Vergini and M. Saraceno, Phys. Rev. E **52**, 2204 (1995).

[8] S. Fishman, in *Quantum Chaos*, Proceedings of the International School of Physics "Enrico Fermi," Course CXIX, edited by G. Casati, I. Guarneri, and U. Smilansky (North-Holland, Amsterdam, 1991).

[9] M. Raizen, in *New Directions in Quantum Chaos*, Proceedings of the International School of Physics "Enrico Fermi," Course CXLIII, edited by G. Casati, I. Guarneri, and U. Smilansky (IOS Press, Amsterdam, 2000).

[10] E. Vergini, Ph.D. thesis, Universidad de Buenos Aires, 1995 (unpublished).

[11] A. Barnett, Ph.D. thesis, Harvard University, 2000 (unpublished).

[12] D.A. Wisniacki and E. Vergini, Phys. Rev. E **59**, 6579 (1999).

[13] D. Cohen, A. Barnett, and E.J. Heller, Phys. Rev. E **63**, 046207 (2001).

[14] D. Cohen, Phys. Rev. Lett. **82**, 4951 (1999).

[15] D. Cohen and T. Kottos, Phys. Rev. Lett. **85**, 4839 (2000).

[16] D. Cohen, Ann. Phys. (N.Y.) **283**, 175 (2000).

[17] D. Cohen, in *New Directions in Quantum Chaos* (Ref. [9]).

[18] A. Barnett, D. Cohen, and E.J. Heller, J. Phys. A **34**, 413 (2001); Phys. Rev. Lett. **85**, 1412 (2000).

[19] D. Cohen, Phys. Rev. E **65**, 026218 (2002).

[20] D. Cohen and T. Kottos, Phys. Rev. E **63**, 036203 (2001).

[21] M. Wilkinson, J. Phys. A **21**, 4021 (1988); **20**, 2415 (1987).

[22] O.M. Auslaender and S. Fishman, Phys. Rev. Lett. **84**, 1886 (2000); J. Phys. A **33**, 1957 (2000).

[23] J.M. Robbins and M.V. Berry, J. Phys. A **25**, L961 (1992); M.V. Berry and J.M. Robbins, Proc. R. Soc. London, Ser. A **442**, 659 (1993); M.V. Berry and E.C. Sinclair, J. Phys. A **30**, 2853 (1997).

[24] M. Feingold and A. Peres, Phys. Rev. A **34**, 591 (1986). M. Feingold, D. Leitner, and M. Wilkinson, Phys. Rev. Lett. **66**, 986 (1991); M. Wilkinson, M. Feingold, and D. Leitner, J. Phys. A **24**, 175 (1991); M. Feingold, A. Gioletta, F. M. Izrailev, and L. Molinari, Phys. Rev. Lett. **70**, 2936 (1993).